Model of PE-CVD apparatus: Verification and Simulations

J.GEISER[1], V.BUCK[2], and M.ARAB[3]

[1]*Humboldt-Universität zu Berlin,Department of Mathematics, Unter den Linden 6, D-10099 Berlin, Germany*

[2]*University of Duisburg-Essen, Department of Physics, Lotharstr.1, D-47048 Duisburg, Germany*

Email: geiser@mathematik.hu-berlin.de

[3]*Humboldt-Universität zu Berlin, Department of Mathematics, Unter den Linden 6, D-10099 Berlin, Germany*

Email: arab@mathematik.hu-berlin.de

ABSTRACT

In this paper we present the simulation of a chemical vapor deposition for metallic bipolar plates.

For chemical vapor deposition, the delicate optimization between temperature, pressure and plasma power is important to obtain a homogeneous deposition, see (Hlavacek and Orlicki 1995).

The aim is to reduce real-life experiments of a given CVD plasma reactor, based on a large physical parameter space we have a hugh amount of experiments.

A detail study of the physical experiments on a CVD plasma reactor allows to reduce to an approximated mathematical model, which is the underlying transport-reaction model.

Significant region of the CVD apparatus are approximated and physical parameters are transferred to the mathematical parameters. Such approximation reduced the mathematical parameter space to a realistic amount of numerical experiments.

Based on interpolation and regression functions we fit to the physical parameter space and can give first prediction to deposition rates with the simulation model.

Here numerical experiments help to understand the deposition process and the control the positions of the sources for the deposition and precursor gases.

For the simulations we apply analytical as well as numerical methods to obtain results to predict the growth of thin layers.

The results are discussed with physical experiments to give a valid model for the assumed growth.

Here an important transfer of engineering research on modelling real-life processes to acchieve a simulatable mathematical model. Such a model can be solved by numerical solvers and discretisation schemes. The resullts can be used to obtain a new understanding of the technical processes in engineering research.

Keywords: Chemical vapor deposition, multi-scale problem, approximation methods, numerical simulation.
AMS subject classifications. 35K25, 35K20, 74S10, 70G65.

1 INTRODUCTION

We motivate our study by simulating a growth of a thin film that can be done by PE-CVD (plasma enhanced chemical vapor deposition) processes, see (Lieberman and Lichtenberg 2005) and (Ohring 2002). Such technical processes are very complex and real-life experiments enormous extensive and expensive. Based on a large physical parameter space the amount of experiments are al least the variation of all possible parameters. Such large numbers of experiments can be reduced to with the help of numerical experiments based on a mathematical model. Such modelling results are based on an interdiciplinary work with engineers, mathematicians and physicists. We derive a multiphysics model, that includes a simplification of the dominant physical processes, i.d. transport of the reactive species in the gas phase and their deposition rates at the target layer.

The approximation between the mathematical parameters and physical parametes can be done with regression method, such that we can verify to the physical experiments. Such an approximations help to study the physical experiments with simulation tools which are more cheaper and can foresee the more appropriate experiments which should be done to understand and control the physical processes.

In the following we introduce the PE-CVD process and its important modelling directions.

A gas exposed to an electric field in low pressure conditions $(< 5$ Torr$)$ results in a non-equilibrium plasma, see (Chapman 1980) and (Morosoff 1990). Such ionized media, known as "cold" plasma or glow discharges, are powerful surface-modification tools in Material Science and Technology. Low-pressure plasmas allow to modify the surface chemistry and properties of materials compatible with low-medium vacuum, through a PE-CVD process, see applications (Favia and D'Agostino 2002) and (Morosoff 1990).

Here PE-CVD processes are attractive methods, because of their reproduceable chemical processes that can be controlled by pressure, by temperature, and by additional precursor gases. Such methods are developed since recent years and are interested on producing high-temperature films, see (Ohring 2002).

We consider models that are related to mesoscopic scales, (Gobbert and Ringhofer 1998), with respect to flows close to the wafer surface, where the wafer is a target material (e.g., metal or ceramic) for the deposition, shortciteohring02. We assume that the wafer is a homogene media and the surface can be modeled as a porous media, (Rouch 2006).

The physical experiments are used to obtain the influence of temperature, pressure and plasma power to the deposition rates, see (Kadetov 2004). Here the plasma reactor chamber of a NIST *GEC reference cell* is used and for the hybrid ICP/CCP-RF plasmasource a double spiral antenna, see (Kadetov 2004), is applied. Such experiments are important but under the variation of all the parameters very extensive.

Mathematically we apply interpolation between the physical and mathematical parameters to verify a simulation model. Based on the smaller mathematical parameter space, we can allow much more experiments and obtain via the regression function the resulting parameters to the

phyical experiments. Such switching between numerical experiments and physical experiments reduce to a possible amount of experiments and we can optimize the deposition process.

The numerical results are discussed and applied to validation problems and real-life problems. We discuss an applications to deposit small films SiC to a metallic plate.

The paper is organized as follows.

In Section 2, we present our mathematical model and a possible reduced model for further approximations. In Section 3, we discuss the physical experiments of the CVD process. The numerical methods of transport-reaction equation and their parameter approximation to the physical model is described in Section 4 The numerical experiments are given in Section 5. In Section 6, we briefly summarize our results.

2 MATHEMATICAL MODEL

In the next we discuss the derivation of the model.

We start with developing the multiphase model in the following steps:

- Standard Transport model (one phase)
- Flow model (flow field of the plasma medium)
- Multiphase model with mobile and immobile zones

In each model part we can refine the processes of the transport for the deposition gaseous species or reaction gaseous species with regard to the influence of flow field, plasma zones and precursor gases.

A schematic test geometry of the CVD reactor is given in Figure 1.

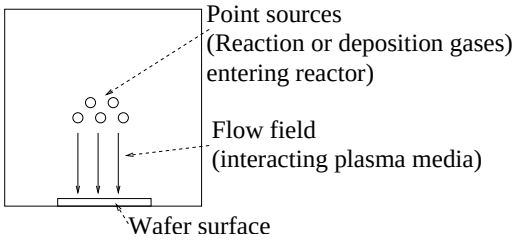

Figure 1: Vertical impinging CVD reactor.

2.1 Standard Transport Model

In the following, the models are discussed in terms of far-field and near-field problems, which take into account the scales of the models.

Two different types of models can be discussed:

1. Convection-diffusion-reaction equations (Gobbert and Ringhofer 1998) (far-field problem);

2. Boltzmann-Lattice equations (Senega and Brinkmann 2006) (near-field problem).

The modeling is governed by a Knudsen Number, whereby the Knudsen number is a dimensionless number and defines the ratio of the molecular mean free path length to a representative physical length scale.

$$Kn = \frac{\lambda}{L}, \tag{1}$$

where λ is the mean free path and L is the representative physical length scale. This length scale could be, for example, the radius of a body in a fluid. Here we deal with small Knudsen Numbers $Kn \approx 0.01 - 1.0$ for a convection-diffusion-reaction equation and a constant velocity field, whereas for large Knudsen Numbers $Kn \geq 1.0$ we deal with a Boltzmann equation (Ohring 2002). From the modeling of the gaseous transport of the deposition species, we consider the pure far-field model and assume a continuum flow field, see (George 2008).

Such assumptions leads to transport equations that can be treated with a convection-diffusion-reaction equation owing to a constant velocity field, see:

$$\frac{\partial}{\partial t}c + \nabla F - R_g = q(x,t), \text{ in } \Omega \times [0,t] \tag{2}$$
$$F = \mathbf{v}c - D\nabla c,$$

$$c(x,t) = c_0(x), \text{ on } \Omega, \tag{3}$$

$$c(x,t) = c_1(x,t), \text{ on } \partial\Omega \times [0,t], \tag{4}$$

where c is the molar concentration of the reaction gases (called species) and F the flux of the species. $\mathbf{v}$ is the flux velocity through the chamber and porous substrate (Rouch 2006). D is the diffusion matrix and R_g is the reaction term. The initial value is given as c_0 and we assume a Dirichlet boundary with the function $c_1(x,t)$ sufficiently smooth. $q(x,t)$ is a source function, depending on time and space, and represents the inflow of the species.

The parameters of the equation are derived as follows. The diffusion in the modified CVD process is given by the Knudsen diffusion, (Cao and Burggraaf 1993). We consider the overall pressure in the reactor is $200\ Pa$ and the substrate temperature (or wafer surface temperature) is about $600 - 900\ K$. The pore size in the homogeneous substrate is assumed to be $80\ nm$. The homogeneous substrate can be either a porous medium, e.g. a ceramic material, see (Cao and Burggraaf 1993) or a dense plasma, assumed to be very dense and stationary, see (Lieberman and Lichtenberg 2005). For such media we can derive the diffusion based on the Knudsen diffusion.

The diffusion is described as:

$$D = \frac{2\epsilon\mu_K\nu r}{3RT}, \tag{5}$$

where ϵ is the porosity, μ_K is the shape factor of the Knudsen diffusion, r is the average pore radius, R and T are the gas constant and temperature, respectively, and ν is the mean molecular

speed, given by:

$$\nu = \sqrt{\frac{8RT}{\pi W}}, \tag{6}$$

where W is the molar mass of the diffusive gas.

For the homogeneous reactions, we consider during the CVD process a constant reaction of Si, Ti and C species given as:

$$3Ti + Si + 2C \rightarrow Ti_3SiC_2, \tag{7}$$

where Si_3TiC_2 is a MAX-phase material, see (Barsoum and El-Raghy 1996), which deposits at the wafer surface. For simplicity, we do not consider the intermediate reaction with the precursor gases, (Lieberman and Lichtenberg 2005) and assume we are dealing with a compound gas $3Ti + Si + 2C$, see (Dobkin and Zuraw 2003). Therefore we can concentrate on one species transport.

The reaction rate is then given by:

$$\lambda = k_r \frac{[3Si]^M [Ti]^N [2C]^O}{[Si_3TiC_2]^L}, \tag{8}$$

where k_r is the apparent reaction constant, L, M, N, O are the reaction orders of the reactants. A schematic overview of the one-phase model is presented in Figure 2. Here the gas chamber of the CVD apparatus is shown, which is modeled by a homogeneous medium.

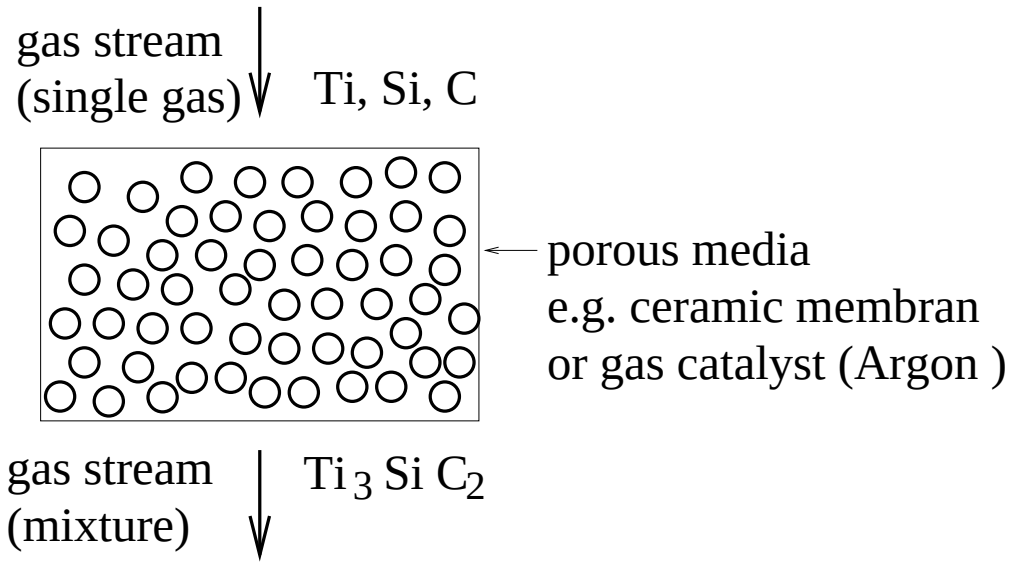

Figure 2: Gas chamber of the CVD apparatus.

2.2 Flow Field

The flow field in which derives the velocity is used for the transport of the species. The velocity in the homogeneous substrate is modeled by a porous medium (Bear 1972; Johannsen 1999). We assume stationary or low reactive medium, e.g. non-ionized or low-ionized plasma or less reactive precursor gas. Further, the pressure can be assumed with the Maxwell distribution as (Lieberman and Lichtenberg 2005):

$$p = \rho b T, \tag{9}$$

where ρ is the density, b is the Boltzmann's constant and T is the temperature.

The model equations are based on mass and momentum conserved equations, where we assume conserved energy conservation. Because of the low temperature and low pressure environment, we assume the gaseous flow has a nearly liquid behavior. Therefore derivation of the velocity can be given by Darcy's law:

$$\boldsymbol{v} = -\frac{k}{\mu}(\nabla p - \rho g)\,, \tag{10}$$

where $\boldsymbol{v}$ is the velocity of the fluid, k is the permeability tensor, μ is the dynamic viscosity, p is the pressure, g is the vector of the gravity and ρ is the density of the fluid.
We use the continuum equation of the particle density and obtain the equation of the system, which is given as our flow equation:

$$\partial_t(\phi\rho) + \nabla \cdot (\rho \boldsymbol{v}) = Q\,, \tag{11}$$

where ρ is the unknown particle density, ϕ is the effective porosity and Q is the source-term of the fluid. We assume a stationary fluid and consider only divergence-free velocity fields, i.e.

$$\nabla \cdot \boldsymbol{v}(x) = 0\,, \quad x \in \Omega\,. \tag{12}$$

The boundary conditions for the flow equation are given as:

$$p = p_r(t,\gamma), \quad t > 0\,, \quad \gamma \in \partial\Omega\,, \tag{13}$$

$$\boldsymbol{n} \cdot \boldsymbol{v} = m_f(t,\gamma), \quad t > 0\,, \quad \gamma \in \partial\Omega\,, \tag{14}$$

where $\boldsymbol{n}$ is the normal unit vector with respect to $\partial\Omega$, where we assume that the pressure p_r and flow concentration m_f are prescribed by Dirichlet boundary conditions (Johannsen 1999).
From the nearly stationary fluids, we assume that the conservation of momentum for velocity $\boldsymbol{v}$ is given (Glowinski 2003; Johannsen 1999). Therefore we can neglect the computation of the momentum for the velocity.

Remark 1 *For the flow through the gas chamber, for which we assume a homogeneous medium and non-reactive plasma, we have considered a constant flow (Hlavacek and Orlicki 1995). A further simplification is given by the very small porous substrate, for which we can assume the underlying velocity in a first approximation as constant (Ohring 2002).*

Remark 2 *For an instationary medium and reactive or ionized plasma, we have to take into account the relations of the electrons in the thermal equilibrium. Such spatial variation can be*

considered by modeling the electron drift. Such modeling of the ionized plasma is done with the Boltzmanns relation, (Lieberman and Lichtenberg 2005).

2.3 Multiphase Model: Mobile and Immobile Zones

More complicated processes such as retardation, adsorption and dissipation processes of the gaseous species are modelled with multiphase equations. We take into account that concentration of species can be given in a mobile and immobile version, depending on their different reactive states, see (**?**). From these behaviours, we have to model a transport and an adsorbed state of the species, see also Figure 3. Here the mobile and immobile phases of the gas concentration are shown in the macroscopic scale of the porous medium.

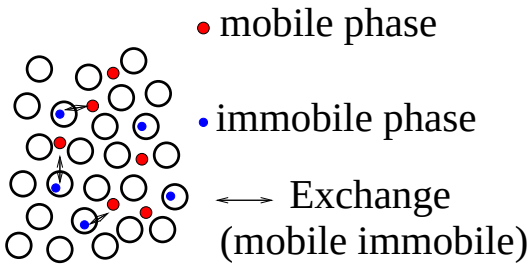

Figure 3: Mobile and immobile phase.

The model equations are given as combinations of transport and reaction equations (coupled partial and ordinary differential equations), given as:

$$\phi\partial_t c_i^L + \nabla\cdot(\mathbf{v}c_i^L - D^{e(i)}\nabla c_i^L) = g(-c_i^L + c_{i,im}^L) - \lambda_{i,i}\phi c_i^L + \sum_{k=k(i)} \lambda_{i,k}\phi c_k^L + \tilde{Q}_i, \qquad (15)$$

$$\phi\partial_t c_{i,im}^L = g(c_i^L - c_{i,im}^L) - \lambda_{i,i}\phi c_{i,im}^L + \sum_{k=k(i)} \lambda_{i,k}\phi c_{k,im}^L + \tilde{Q_{i,im}},$$

ϕ : effective porosity $[-]$,

c_i^L : concentration of the ith gaseous species in the plasma chamber

$c_{i,im}^L$: concentration of the ith gaseous species in the immobile zones of the plasma chamber phase $[mol/mm^3]$,

$\mathbf{v}$: velocity in the plasma chamber $[mm/nsec]]$,

$D^{e(i)}$: element-specific diffusions-dispersions tensor $[mm^2/nsec]]$,

$\lambda_{i,i}$: decay constant of the ith species $[1/nsec]]$,

$\tilde{Q}_i$: source term of the ith species $[mol/(mm^3 nsec)]$,

g : exchange rate between the mobile and immobile concentration $[1/nsec]$,

where $i = 1, \ldots, M$ and M denotes the number of components.

The parameters in Equation (15) are further described, see also (Geiser 2003).
The effective porosity is denoted by ϕ and describes the portion of the porosities of the aquifer that is filled with plasma, and we assume a nearly fluid phase. The transport term is indicated by the Darcy velocity $\mathbf{v}$, that presents the flow-direction and the absolute value of the plasma flux. The velocity field is divergence-free. The decay constant of the ith species is denoted by λ_i. $k(i)$ therefore denotes the indices of the other species.

Remark 3 *The concentrations in the mobile zones are modeled with convection-diffusion-reaction equations, see also subsection 2.1, where the concentration in the immobile zones are modeled with reaction equations. These two phases present mobility of the gaseous species through the homogeneous media, where the concentrations in the immobile zones are at least lost amounts of depositable gases.*

2.4 Simplified model: Far-Field Model

We concentrate on a far-field model and assume a continuum flow, and that the transport equations can be treated with a convection-diffusion-reaction equation, due to a constant velocity

field, see:

$$\frac{\partial}{\partial t}c + \nabla F - R_g = 0, \text{ in } \Omega \times [0,t] \tag{16}$$

$$F = \mathbf{v}c - D\nabla c,$$

$$c(x,t) = c_0(x), \text{ on } \Omega, \tag{17}$$

$$c(x,t) = c_1(x,t), \text{ on } \partial\Omega \times [0,t], \tag{18}$$

where c is the molar concentration and F the flux of the species. $\mathbf{v}$ is the flux velocity through the chamber and porous substrate (Rouch 2006). D is the diffusion matrix and R_g is the reaction term. The initial value is given as c_0 and we assume a Dirichlet boundary with the function $c_1(x,t)$ sufficiently smooth.

Remark 4 *The concentration to only dominant far field processes in the gas phase to the reactive species reduces enormously the physical parameter space. Such a realistic reduction with respect to the experiments can reduce also the underlying mathematical model and concentrate on a defined number of experiments. Such experiments can validate the switching between the phyical and mathematical parameter space and allows to foresee the important processes in the gas phase.*

3 PHYSICAL EXPERIMENTS

Base of the experimental setup is the plasma reactor chamber of a NIST *GEC reference cell*. The spiral antenna of the hybrid ICP/CCP-RF plasmasource was replaced by a double spiral antenna (Kadetov 2004). This reduce the asymmetry of the magnetic field due to superposition of the induced fields of both antennas. Also the power coupling to the plasma increase and enhance the efficiency of the source. A set of MKS massflowcontrollers allow any defined mixture of gaseous precursors. Even the flows of liquid precursors with high vapor pressure is controlled by this system. All other liquid and all solid precursors will direct transported to the chamber by controlled carrier gas flow. Beside the precursor flow, also the density can be changed by variation of pressure inside the recipient. Control to the pressure is given due

to a valve between the recipient and the vacuum-pumps. Additional a heated and insulated substratholder was mounted. Hereby a temperature up to 800^oC and a bias voltage can be applied to the substrate. While pressure and RF power determine the undirected particle energy (plasmatemperature) , the bias voltage adds, only to charged particles, energy directed at the Substrate. Aside the pressure and RF power control the grade of ionization and the number as well as the size of molecular fractions.

Altogether this setup provide as free process parameters:

- Pressure (typical $10^{-1} - 10^{-2}$ mbar)
- Precursor-composition (TMS, $TMS + H_2$, $TMS + O_2$)
- Precursor flow-rate (range form SCCM up to SLM)
- RF-Power (up to 1100W)
- Substrate temperature (RT - 800^oC)
- Bias voltage (DC, unipolar and bipolar pulsed, floating)

During all experiments the process was observed with optical emission spectroscopy (OES) and mass spectroscopy (MS). The stoichiometry of deposited films was ex situ analyzed on a scanning electron microscope (SEM) by energy dispersive X-ray analysis (EDX).

Realisation of the Physical Experiments

The following parameters are used for the physical experiments. Such reduction allows to concentrate on important flow and transport processes in the gas phase. Further we apply the underlying mathematical model (fare field model, see Subsection 2.4) such that we can switch between the physical and mathematical parameters.

Precursor: Tetramethylsilan (TMS)
Substrate: VA-Steel

Film at the substrate : $Si\,C_x$

Test	P_R [mbar]	ϑ_S [C]	P_{Plasma} [W]	ϕ(TMS) [SCCM]	$\phi(H_2)$ [SCCM]	Ratio [C:Si]	Mass (growth) [g]	Zeit [min]
080701-01-VA	9.7E-2	400	900	10.23	0	0.97811	0.00012	120
080718-01-VA	1.1E-1	400	900	10.00	0	1.00174	0.00050	130
080718-02-VA	4.5E-2	400	900	10.00	0	1.24811	0.00070	110
080618-01-VA	4.3E-2	400	500	10.23	0	1.32078		127
080716-01-VA	1.1E-1	400	500	10.00	0	1.42544	0.00250	120
080715-02-VA	1.1E-1	400	100	10.00	0	1.58872	0.00337	122
080804-01-VA	4.5E-2	400	100	10.00	0	2.91545	0.00356	129
080630-01-VA	9.9E-2	800	900	10.23	0	1.09116	0.00102	120
080807-01-VA	4.5E-2	800	900	10.00	0	1.18078	0.00118	120
080625-01-VA	3.9E-2	800	500	10.23	0	1.06373		120
080626-01-VA	9.3E-2	800	500	10.23	0	1.12818	0.00174	130
080806-01-VA	4.8E-2	800	100	10.00	0	1.73913	0.00219	121
080715-01-VA	1.1E-1	800	100	10.00	0	1.62467	0.00234	120
081016-01-VA	1.0E-1	600	300	10.00	0	1.72898	0.00321	123
081020-01-VA	1.1E-1	600	300	10.00	50	1.49075	0.00249	114
081028-01-VA	1.1E-1	600	300	10.00	15	1.53549	0.00273	120
081023-01-VA	1.1E-1	600	300	10.00	10	1.54278	0.00312	127
081027-01-VA	1.1E-1	600	300	10.00	5.5	1.55818	0.00277	126
081024-01-VA	1.1E-1	600	300	10.00	3.5	1.64367	0.00299	120
081022-01-VA	1.0E-1	600	300	10.00	2.5	1.69589	0.00318	127

We apply the following parameters for the interpolation of the substrate temperature we use:

Temperature	Ratio(SiC:C)
400	2.4:1
600	1.5:1
700	1.211:1
800	1.1:1

for the substrate temperature and the power of the plasma we use:

Temperature [C]	Power [W]	Ratio(SiC:C)
400	900	1:0.97
400	500	1.3:1
800	900	1.18:1

Remark 5 *For the process the temperature and power of the plasma is important and experiments show these significant parameters. Based on these parameters we initialize the mathematical model and interpolate the flux and reaction parts.*

4 NUMERICAL METHODS

In this section we discuss the numerical methods. To accelerate our numerical methods, we combined numerical and analyical parts in the solver processes.

4.1 Discretization and Solver Methods

For the space-discretization of the PDE's we apply finite-volume methods as mass conserved discretization schemes and for the time-discretization of resulting ODE's we apply Runge-Kutta methods or BDF methods. To accelerate the solver process, we combine numerical and analytical parts of the solutions.

4.1.1 Discretization method of the convection equation

We deal with the following convection equation

$$\partial_t R\, c - \mathbf{v} \cdot \nabla c = 0 \;, \tag{19}$$

where R is the retardation factor, and presents the retention of the concentration, see also equation (16). $\mathbf{v}$ is the velocity. We have a simple boundary condition $c = 0$ for the inflow and outflow boundary and the initial values are given as $c(x_j, 0) = c_j^0(x)$. We use piecewise constant discretization method with the upwind discretization done in (Frolkovič and Geiser 2003) and get

$$\begin{aligned} V_j\; R\; c_j^{n+1} &= V_j\; R\; c_j^n - \tau^n \sum_{k \in out(j)} v_{jk}\; c_j^n \; + \tau^n \sum_{k \in in(j)} c_k^n\; v_{kj} \;, \\ V_j\; R\; c_j^{n+1} &= c_j^n (R\; V_j - \tau^n \nu_j) + \tau^n \sum_{k \in in(j)} c_k^n\; v_{kj} \;, \end{aligned} \tag{20}$$

The explicit time discretization has to fulfill the discrete minimum-maximum property (Frolkovič and Geiser 2003), and we get the following restriction for the time steps

$$\tau_j = \frac{R\; V_j}{\nu_j} \;, \quad \tau^n \leq \min_{j=1,\ldots,I} \tau_j \;. \tag{21}$$

To obtain improved spatial discretization methods and apply larger time-steps, we introduce a reconstruction with linear polynomials as a higher test-function in the next subsection.

4.1.2 Discretization method for the convection-reaction equation based on embedded one dimensional analytical solutions

We apply Godunovs method for the discretization method, cf. (Leveque 2002), and extend the formulation with analytical solution of convection-reaction equations. We reduce the multi-dimensional equation to one dimensional equations and solve each equation exactly. The one-dimensional solution is multiplied with the underlying volume and we get the mass-formulation. The one-dimensional mass is embedded into the multi-dimensional mass-formulation and we obtain the discretization of the multi-dimensional equation.

The algorithm is given in the following manner

$$\partial_t \; c_l + \nabla \cdot \mathbf{v}_l \; c_l = -\lambda_l \; c_l + \lambda_{l-1} \; c_{l-1},$$

with $l = 1, \ldots, m$.

The velocity vector $\mathbf{v}$ is divided by R_l. The initial conditions are given by $c_1^0 = c_1(x, 0)$, else $c_l^0 = 0$ for $l = 2, \ldots, m$ and the boundary conditions are trivial $c_l = 0$ for $l = 1, \ldots, m$.

We first calculate the maximal time step for cell j and concentration i with the use of the total outflow fluxes

$$\tau_{i,j} = \frac{V_j \; R_i}{\nu_j} \; , \quad \nu_j = \sum_{k \in out(j)} v_{jk} \; .$$

We get the restricted time step with the local time steps of cells and their components

$$\tau^n \leq \min_{\substack{i=1,\ldots,m \\ j=1,\ldots,I}} \tau_{i,j} \; .$$

The velocity of the discrete equation is given by

$$v_{i,j} = \frac{1}{\tau_{i,j}} \ .$$

We calculate the analytical solution of the mass, cf. (Geiser 2003) and we get

$$\begin{aligned} m^n_{i,jk,out} &= m_{i,out}(a, b, \tau^n, v_{1,j}, \ldots, v_{i,j}, R_1, \ldots, R_i, \lambda_1, \ldots, \lambda_i) \ , \\ m^n_{i,j,rest} &= m^n_{i,j} \ f(\tau^n, v_{1,j}, \ldots, v_{i,j}, R_1, \ldots, R_i, \lambda_1, \ldots, \lambda_i) \ , \end{aligned}$$

where $a = V_j R_i (c^n_{i,jk} - c^n_{i,jk'})$, $b = V_j R_i c^n_{i,jk'}$ and $m^n_{i,j} = V_j R_i c^n_{i,j}$. Further $c^n_{i,jk'}$ is the concentration at the inflow- and $c^n_{i,jk}$ is the concentration at the outflow-boundary of the cell j.

The discretization with the embedded analytical mass is calculated by

$$m^{n+1}_{i,j} - m^n_{i,rest} = - \sum_{k \in out(j)} \frac{v_{jk}}{\nu_j} \ m_{i,jk,out} + \sum_{l \in in(j)} \frac{v_{lj}}{\nu_l} \ m_{i,lj,out} \ ,$$

where $\frac{v_{jk}}{\nu_j}$ is the re-transformation for the total mass $m_{i,jk,out}$ in the partial mass $m_{i,jk}$. In the next time-step the mass is given as $m^{n+1}_{i,j} = V_j \ c^{n+1}_{i,j}$ and in the old time-step it is the rest mass for the concentration i. The proof is done in (Geiser 2003). In the next section we derive an analytical solution for the benchmark problem, cf. (Higashi and Pigford 1980), (Jury and Roth 1990).

In the next subsection we introduce the discretization of the diffusion-dispersion-equation.

4.1.3 Discretization of the diffusion-dispersion-equation

We discretize the diffusion-dispersion-equation with implicit time-discretization and finite-volume method for the following equation

$$\partial_t R\, c - \nabla \cdot (D \nabla c) = 0 \ , \tag{22}$$

where $c = c(x,t)$ with $x \in \Omega$ and $t \geq 0$. The diffusions-dispersions-tensor $D = D(x, \mathbf{v})$ is given by the Scheidegger-approach, cf. (Scheidegger 1961). The velocity is given as $\mathbf{v}$. The retardation-factor is $R > 0.0$.

The boundary-values are denoted by $\mathbf{n} \cdot D\ \nabla c(x,t) = 0$, where $x \in \Gamma$ is the boundary $\Gamma = \partial\Omega$, cf. (Frolkovič 2002). The initial conditions are given by $c(x,0) = c_0(x)$.

We integrate the equation (22) over space and time and derive

$$\int_{\Omega_j} \int_{t^n}^{t^{n+1}} \partial_t R(c)\ dt\ dx = \int_{\Omega_j} \int_{t^n}^{t^{n+1}} \nabla \cdot (D \nabla c)\ dt\ dx \ . \tag{23}$$

The time-integration is done by the backward-Euler method and the diffusion-dispersion term is lumped, cf. (Geiser 2003)

$$\int_{\Omega_j} (R(c^{n+1}) - R(c^n))\ dx = \tau^n \int_{\Omega_j} \nabla \cdot (D \nabla c^{n+1})\ dx \ , \tag{24}$$

The equation (24) is discretized over the space with respect of using the Green's formula.

$$\int_{\Omega_j} (R(c^{n+1}) - R(c^n))\ dx = \tau^n \int_{\Gamma_j} D\ \mathbf{n} \cdot \nabla c^{n+1}\ d\gamma \ , \tag{25}$$

where Γ_j is the boundary of the finite-volume cell Ω_j. We use the approximation in space, confer (Geiser 2003).

The spatial-integration for (25) is done by the mid-point rule over the finite boundaries and given as

$$V_j R(c_j^{n+1}) - V_j R(c_j^n) = \tau^n \sum_{e \in \Lambda_j} \sum_{k \in \Lambda_j^e} |\Gamma_{jk}^e| \mathbf{n}_{jk}^e \cdot D_{jk}^e \nabla c_{jk}^{e,n+1} \ , \tag{26}$$

where $|\Gamma_{jk}^e|$ is the length of the boundary-element Γ_{jk}^e. The gradients are calculated with the piecewise finite-element-function ϕ_l, see ((**?**)) and we obtain

$$\nabla c_{jk}^{e,n+1} = \sum_{l \in \Lambda^e} c_l^{n+1} \nabla \phi_l(\mathbf{x}_{jk}^e) \ . \tag{27}$$

We get with the difference-notation for the neighbor-point j and l, cf. (Frolkovič and De Schepper 2001) and get the discretized equation

$$\begin{aligned} &V_j R(c_j^{n+1}) - V_j R(c_j^n) = \\ &= \tau^n \sum_{e \in \Lambda_j} \sum_{l \in \Lambda^e \setminus \{j\}} \Big(\sum_{k \in \Lambda_j^e} |\Gamma_{jk}^e| \mathbf{n}_{jk}^e \cdot D_{jk}^e \nabla \phi_l(\mathbf{x}_{jk}^e) \Big) (c_j^{n+1} - c_l^{n+1}) \ , \end{aligned} \tag{28}$$

where $j = 1, \ldots, m$.

4.2 Interpolation and regression of experimental dates

To simulate the physical experiments with the assumed model, we have to approximate the parameters of the numerical model. We apply interpoation and regression schemes to approximate between the mathematical and physical parameters.

Here we concentrate on the reaction rates of the species Si, C and H.

The physical dates of temperature and pressure are used and validation simulations done to obtain the ratio of the deposition.

Next we have to interpolate the parameters of the numerical model.

1.) Lagrangian Interpolation:

We assume an interpolation at $\Omega = [a_1, b_1] \times \ldots \times [a_d, b_d]$.

$$T = \sum_{\nu \in K} f(x_\nu^t) L_\nu^t, \tag{29}$$

where the Lagrangian function is given as:

$$L_\nu^t(x) = \pi_{i=1}^d \pi_{\mu=0, \mu \neq \nu_i}^m \frac{x_i - x_\mu^{[a_i, b_i]}}{x_{\nu_i^{[a_i, b_i]}} - x_{\mu^{[a_i, b_i]}}}, \tag{30}$$

2.) Linear Regression (Least square Approximation):

Here we have a points with values and we assume to have a best approximation with respect to minimize:

$$S = \sum_{k=1}^{m} (y_k - L_n(x_k))^2, \tag{31}$$

where $m \geq n$ and L_n is a function that is constructed with the least square algorithm, see (Burlisch and Stoer 2002).

Remark 6 *To apply larger parameter spaces, we can generalise to multivariate regression methods, see (Neil 2002). Here we compute approximations between higher dimensional matrices spaces.*

5 NUMERICAL EXPERIMENTS

For all the experiments we have the following parameters of the model, the discretization and solver methods.

We apply interpolation and regression methods to couple the physical parameters to the mathematical parameters, see Figure 4 and Table 1.

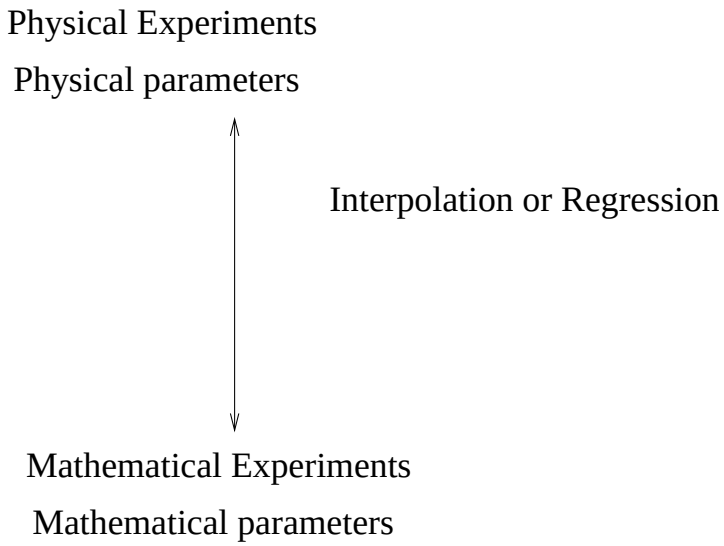

Figure 4: Coupling of physical and mathematical parameter space.

Physical parameter	Mathematical parameter
Temperature,pressure,power T , p , W	velocity, Diffusion,Reaction V , D , λ

Table 1: Physical and mathematical parameters.

Parameters of the equation:

In the following, we have list the parameters for our simulation tool UG, see (Bastian and Rentz-Reichert 1997). The software toolbox has a flexible user interface to allow a large number of numerical experiments and approximate to the known physical parameters.

density	$\rho = 1.0$
mobile porosity	$\phi = 0.333$
immobile porosity	0.333
Diffusion	$D = 0.0$
longitudinal Dispersion	$\alpha_L = 0.0$
transversal Dispersion	$\alpha_T = 0.00$
Retardation factor	$R = 10.0e - 4$ (Henry rate).
Velocity field	$\boldsymbol{v} = (0.0, -4.0\ 10^{-8})^t$.
Decay rate of the species of 1st EX	$\lambda_{AB} = 1\ 10^{-68}$.
Decay rate of the species of 2nd EX	$\lambda_{AB} = 2\ 10^{-8}$, $\lambda_{BNN} = 1\ 10^{-68}$.
Decay rate of the species of 3rd EX	$\lambda_{AB} = 0.25\ 10^{-8}$, $\lambda_{CB} = 0.5\ 10^{-8}$.
Geometry (2d domain)	$\Omega = [0, 100] \times [0, 100]$.
Boundary	Neumann boundary at top, left and right boundaries. Outflow boundary at the bottom boundary

Table 2: Model-Parameters.

Discretization method:

Finite volume method of 2nd order:

spatial step size	$\Delta x_{min} = 1.56, \Delta x_{max} = 2.21$
refined levels	6
Limiter	Slope limiter
Test functions	linear test function reconstructed with neighbor gradients

Table 3: Spatial discretization parameters.

Time discretization methods :

Crank-Nicolson method (2nd order):

Solver method :

In the following, we deal with the test examples which are approximated to the physical experiments.

Initial time-step	$\Delta t_{init} = 5\ 10^7$
controlled time-step	$\Delta t_{max} = 1.298\ 10^7, \Delta t_{min} = 1.158\ 10^7$
Number of time-steps	$100, 80, 30, 25$
Time-step control	time steps are controlled with the Courant-Number $\text{CFL}_{max} = 1$

Table 4: Spatial discretization parameters.

Solver	BiCGstab (Bi conjugate gradient method)
Preconditioner	geometric Multi-grid method
Smoother	Gauss-Seidel method as smoothers for the Multi-grid method
Basic level	0
Initial grid	Uniform grid with 2 elements
Maximum Level	6
Finest grid	Uniform grid with 8192 elements

Table 5: Solver methods and their parameters.

5.1 Test experiment 1: Interpolation with Temperature

In the test example we deal with the following reaction:

$2SiC + 4H \rightarrow_\lambda SiC + CH4 + Si.$

Here we have the physical experiments and approximate to the temperature parameters of $T = 400, 600, 800$.

We computed the ratio $SiC : C$ for the given temperature $T = 400, 600, 800$ with the UG program and fit to the parameter λ.

We used Lagrangian formula to compute λ for the new temperatures $T = 500, 700$ and apply the ratio of the simulated new parameters. This values can be given back to the physical experiments, see Table 6.

One Source

In Figure 5, we present the concentration of the one point source at (50,20).with number of time-steps equal to 25.

T	λ (fitted)	λ (interpolated)	Ratio(SiC:C) (computed with UG)
400	$1/2\ 10^{-8}$		2.4:1
500		$0.35\ 10^{-8}$	1.85:1
600	$1/4\ 10^{-8}$		1.5:1
700		$0.171\ 10^{-8}$	1.211:1
800	$1/8\ 10^{-8}$		1.1:1

Table 6: Computed and experimental fitted parameters with UG simulations.

Point source at the position	$(x, y) = (50, 20)$
Starting point of the source concentration	$t_{start} = 0.0$
End point of the source concentration	$t_{end} = 110^8$
Amount of the permanent source concentration	$c_{source} = 1.0$
Number of time steps	25

Table 7: Parameter of the source concentration.

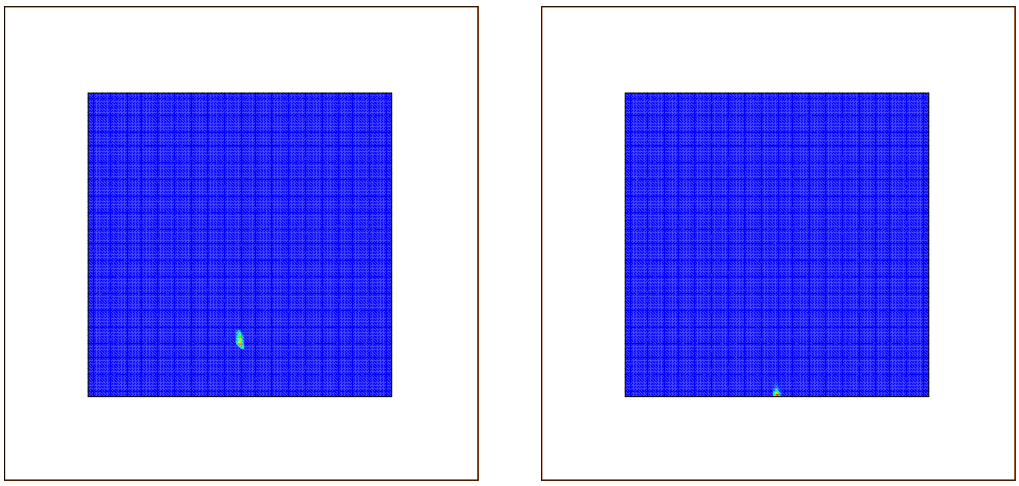

Figure 5: one point source at (50,20) , with number of time-steps equal to 25.

In Figure 6, we show the deposition rates of the one point source at (50,20), with number of time-steps equal to 25.

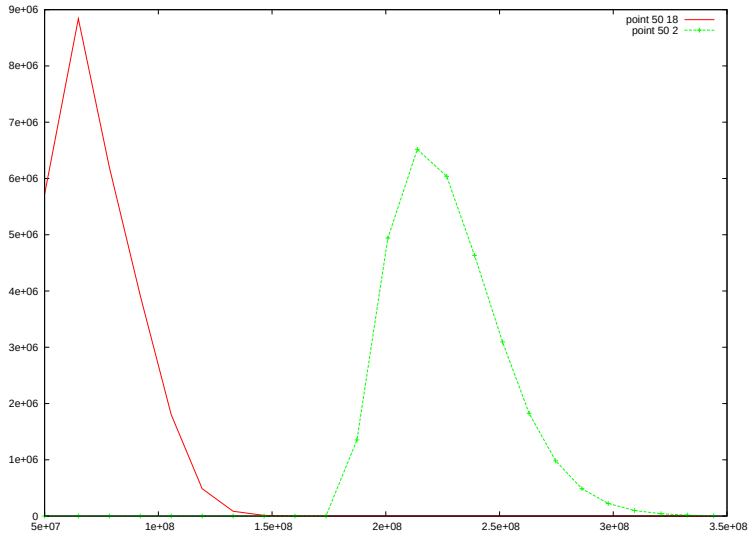

Figure 6: Deposition rates in case of one point source at (50,20), with number of time-steps equal to 25.

Point source at the position	$(x, y) = (50, 20)$
Starting point of the source concentration	$t_{start} = 0.0$
End point of the source concentration	$t_{end} = 110^8$
Amount of the permanent source concentration	$c_{source} = 1.0$
Number of time steps	25

Table 8: Parameter of the source concentration.

RATE
$SiC_{source,max} : SiC_{target,max}$
$9.10^6 : 6.5.10^6 = 1.38$

Table 9: Rate of the concentration.

Nine Point Sources

In this experiment, we apply nine point sources.

In Figure 7, we present the concentration of the nine point sources with short time.

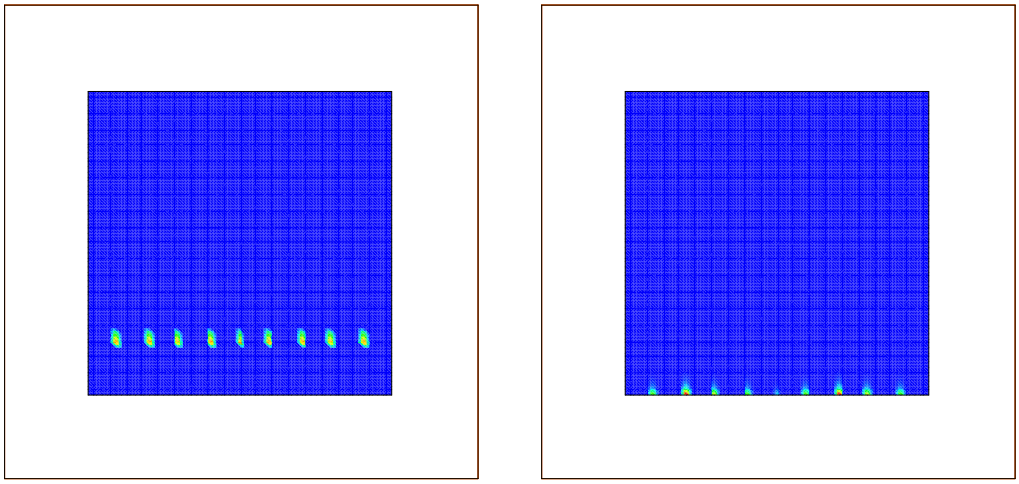

Figure 7: nine point sources, with number of time-steps equal to 25.

In Figure 8, we show the deposition rates of the nine point sources, with number of time-steps equal to 25.

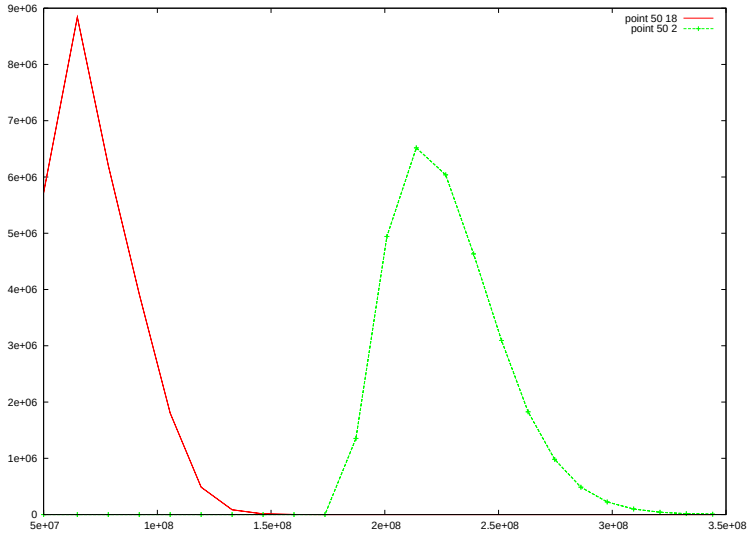

Figure 8: Deposition rates in case of nine point sources, with number of time-steps equal to 25.

RATE
$SiC_{source,max} : SiC_{target,max}$
$9.10^6 : 6.7.10^6 = 1.34$

Table 10: Rate of the concentration.

81 Point Sources

81 point sources at the position	$X = 10, 11, 12, 000, 90. Y = 20.$
Starting point of the source concentration	$t_{start} = 0.0$
End point of the source concentration	$t_{end} = 110^8$
Amount of the permanent source concentration	$c_{source} = 1.0$
Number of time steps	80

Table 11: Parameter of the source concentration.

In this experiment, we apply 81 point sources.

In Figure 9, we present the concentration of the 81 point sources.

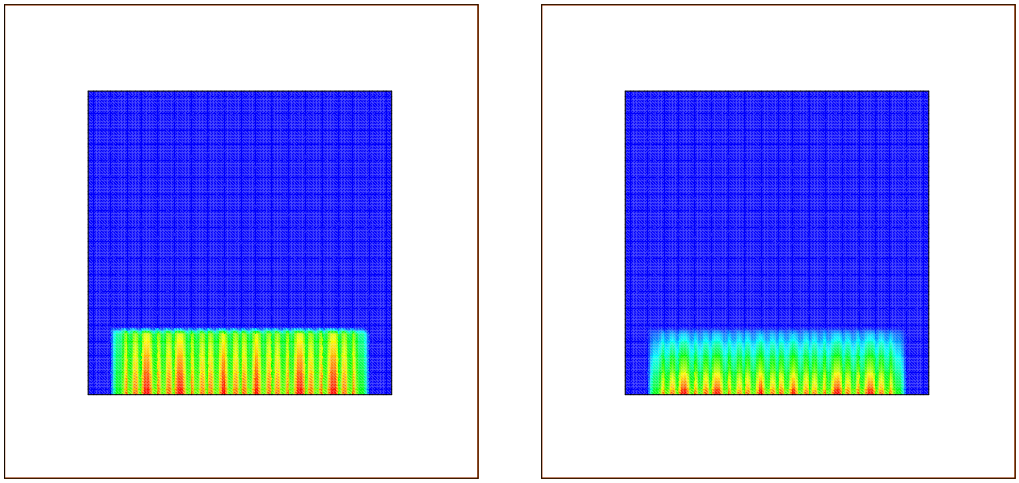

Figure 9: 81 point sources, with number of time-steps equal to 80.

In Figure 10, we show the deposition rates of the 81 point sources, with number of time-steps equal to 80.

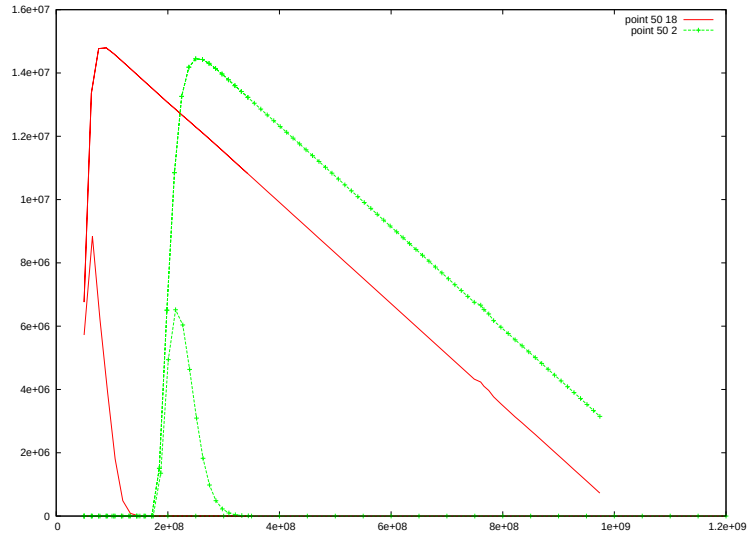

Figure 10: Deposition rates in case of 81 point sources, with number of time-steps equal to 80.

RATE
$SiC_{source,max} : SiC_{target,max}$ $1.5.10^7 : 1.5.10^7 = 1$

Table 12: Rate of the concentration.

Line source

Line source at the position	$x \in [5, 95], y \in [20, 25]$
Starting point of the source concentration	$t_{start} = 0.0$
End point of the source concentration	$t_{end} = 110^8$
Amount of the permanent source concentration	$c_{source} = 1.0$
Number of time steps	25

Table 13: Parameter of the source concentration.

In this part we will make an experiments with line source.

In Figure 11, we present the result of the line source, $x \in [5, 95], y \in [20, 25]$ with number of time steps equal to 25.

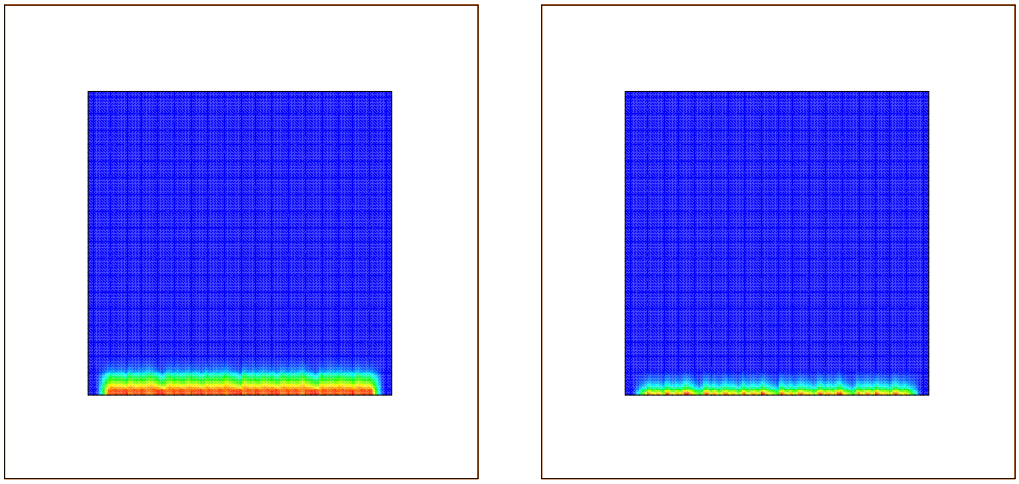

Figure 11: line source, with number of time-steps equal to 25.

In Figure 12, we see the deposition rates of the line source, x is between 5 to 95, and y is between 20 to 25.

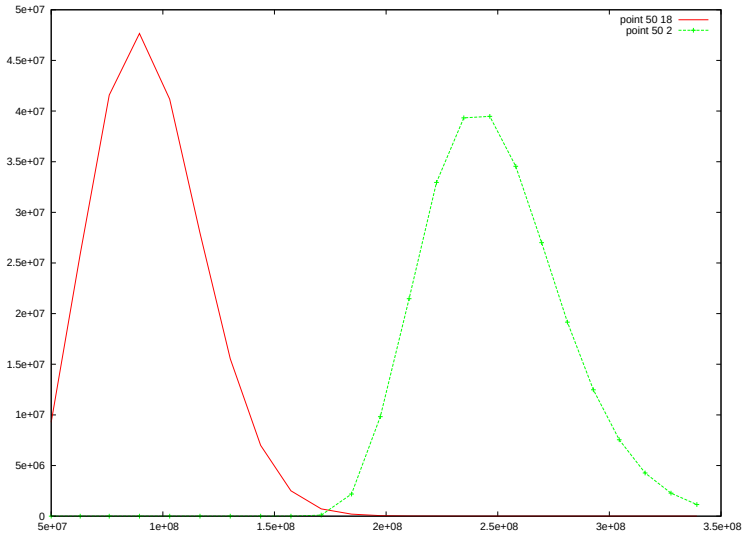

Figure 12: Deposition rates in case of line source, $x \in [5, 95], y \in [20, 25]$.

RATE
$SiC_{source,max} : SiC_{target,max}$
$4.7.10^7 : 4.10^7 = 1.17$

Table 14: Rate of the concentration.

5.2 Test experiment 2: Interpolation with Temperature and Power

In the next experiment, we apply fit the mathematical parameters to the temperature and power of the physical experiments.

We deal with the reaction:

$2SiC + 4H \rightarrow_{\lambda} SiC + CH4 + Si.$

In this case we have a table which has the values of temperature and the power of the plasma and the ratio between the sources.

We have to interpolate the λ to the physical parameters temperature T and power of plasma P. In Table 15 the interpolated parameters are given.

T	P	λ	Ratio(SiC:C)	Computed Ratio
400	900	S. $1/10\ 10^{-8}$	F.1:0.97	1.01
400	500	S. $1/5\ 10^{-8}$	F.1.3:1	1.33
400	100	$1/2\ 10^{-8}$	C.2.4:1	
600	300	$1/4\ 10^{-8}$	C.1.5:1	
800	500	$1/8\ 10^{-8}$	C.1:1	
800	900	S.$1/5.7\ 10^{-8}$	F.1.18:1	1.252

Table 15: Computed (C) and experimental fitted (F) parameters with UG simulations.

One Source

Point source at the position	$(x, y) = (50, 20)$
Starting point of the source concentration	$t_{start} = 0.0$
End point of the source concentration	$t_{end} = 110^8$
Amount of the permanent source concentration	$c_{source} = 1.0$
Number of time steps	25

Table 16: Parameter of the source concentration.

In Figure 13, we present the concentration of the one point source at (50,20).with number of time-steps equal to 25.

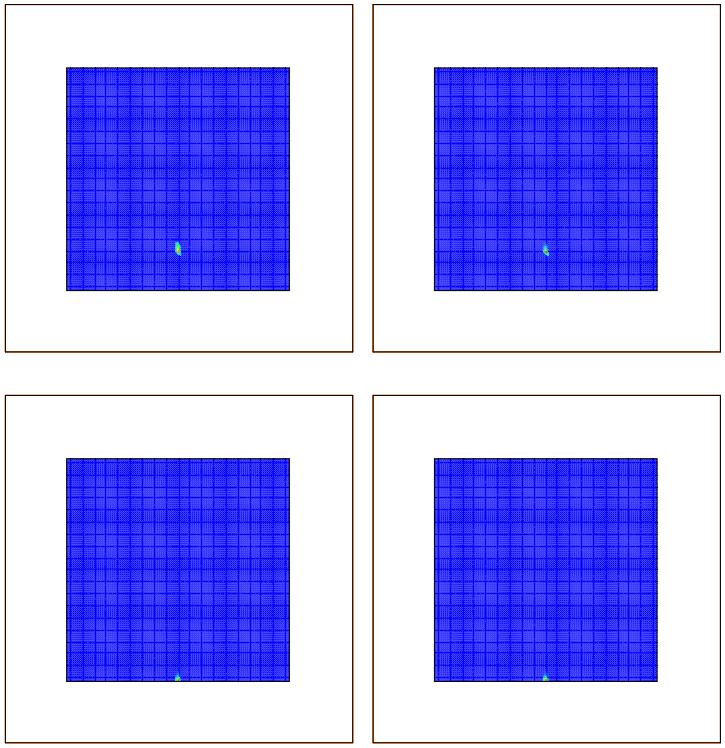

Figure 13: one point source at (50,20) , with number of time-steps equal to 25.

In Figure 14, we show the deposition rates of the one point source at (50,20), with number of time-steps equal to 25.

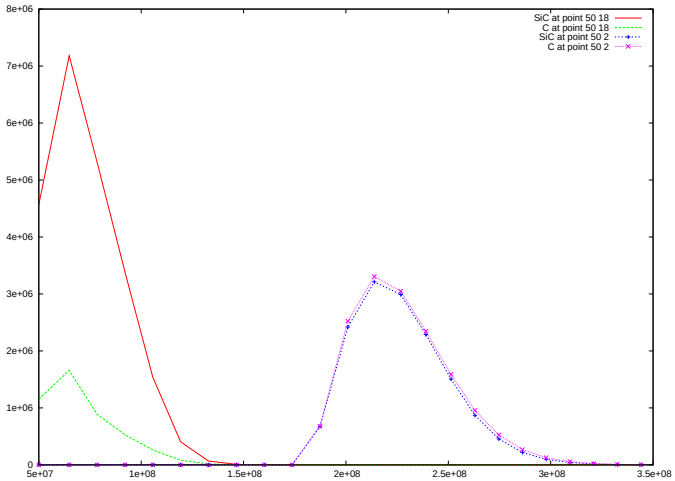

Figure 14: Deposition rates in case of one point source at (50,20), with number of time-steps equal to 25.

RATE
$SiC_{source,max} : C_{target,max}$ $3.10^6 : 3.10^6 = 1$

Table 17: Rate of the concentration.

Nine Point Sources

Nine point sources at the position	$(x = 10, 20, 30, 40, 50, 60, 70, 80, 90.y = 20)$
Starting point of the source concentration	$t_{start} = 0.0$
End point of the source concentration	$t_{end} = 110^8$
Amount of the permanent source concentration	$c_{source} = 1.0$
Number of time steps	25

Table 18: Parameter of the source concentration.

In this experiment, we apply nine point sources.

In Figure 15, we present the concentration of the nine point sources with short time.

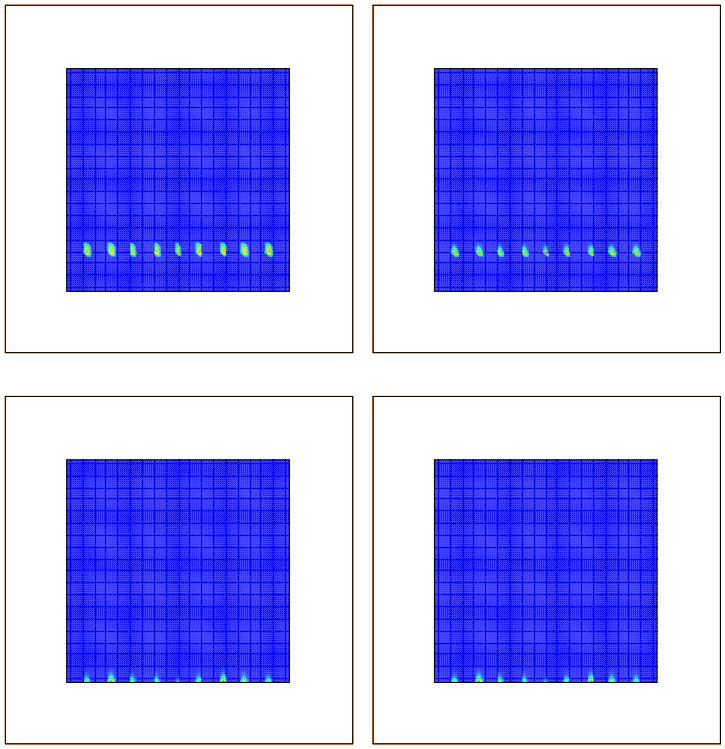

Figure 15: nine point sources, with number of time-steps equal to 25.

In Figure 16, we show the deposition rates of the nine point sources, with number of time-steps

equal to 25.

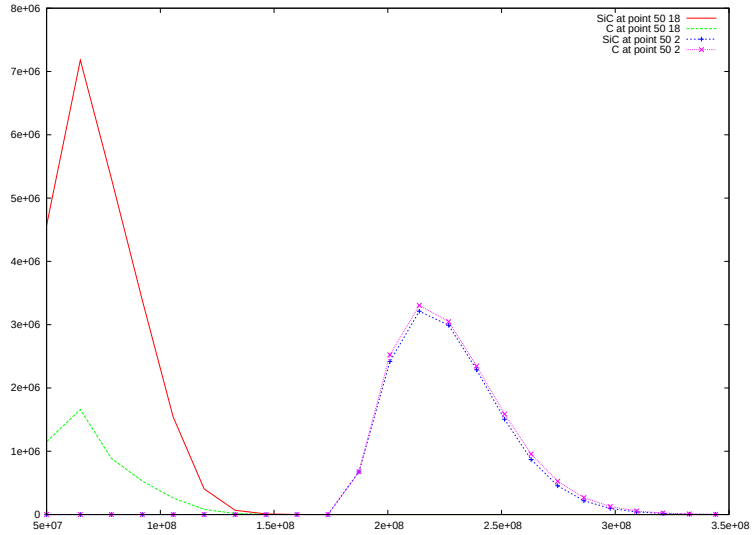

Figure 16: Deposition rates in case of nine point sources, with number of time-steps equal to 25.

RATE
$SiC_{source,max} : C_{target,max}$ $3.10^6 : 3.10^6 = 1$

Table 19: Rate of the concentration.

81 Point Sources

81 point sources at the position	$X = 10, 11, 12, 000, 90. Y = 20.$
Starting point of the source concentration	$t_{start} = 0.0$
End point of the source concentration	$t_{end} = 110^8$
Amount of the permanent source concentration	$c_{source} = 1.0$
Number of time steps	100

Table 20: Parameter of the source concentration.

In this experiment, we apply 81 point sources.

In Figure 17, we present the concentration of the 81 point sources.

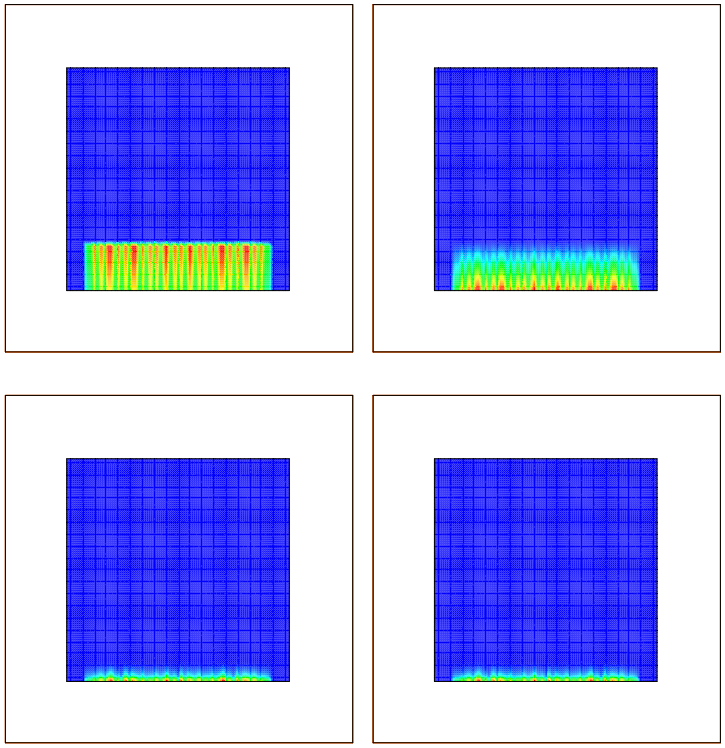

Figure 17: 81 point sources, with number of time-steps equal to 100.

In Figure 18, we show the deposition rates of the 81 point sources, with number of time-steps equal to 100.

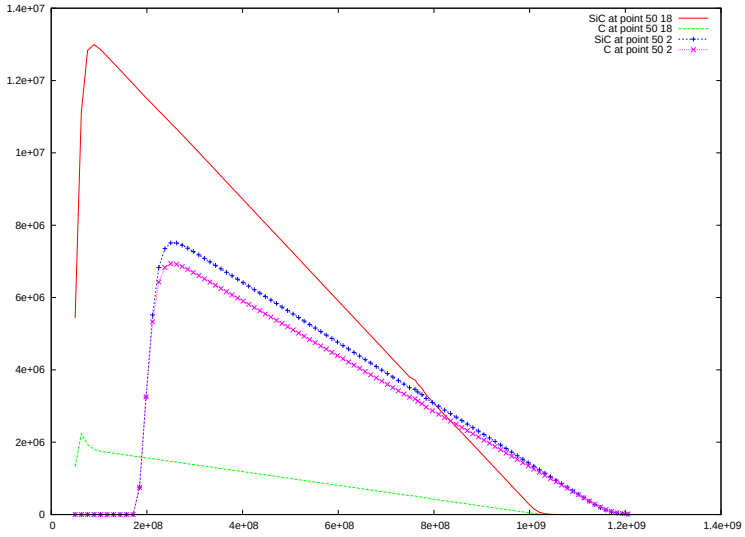

Figure 18: Deposition rates in case of 81 point sources, with number of time-steps equal to 100.

RATE
$SiC_{source,max} : C_{target,max}$ $7.5.10^6 : 7.10^6 = 1.07$

Table 21: Rate of the concentration.

Line source

Line source at the position	$x \in [5, 95], y \in [20, 25]$
Starting point of the source concentration	$t_{start} = 0.0$
End point of the source concentration	$t_{end} = 110^8$
Amount of the permanent source concentration	$c_{source} = 1.0$
Number of time steps	25

Table 22: Parameter of the source concentration.

In this part we will make an experiments with line source, $x \in [5, 95], y \in [20, 25]$.

In Figure 19, we present the result of the line source, $x \in [5, 95], y \in [20, 25]$ with number of time steps equal to 30.

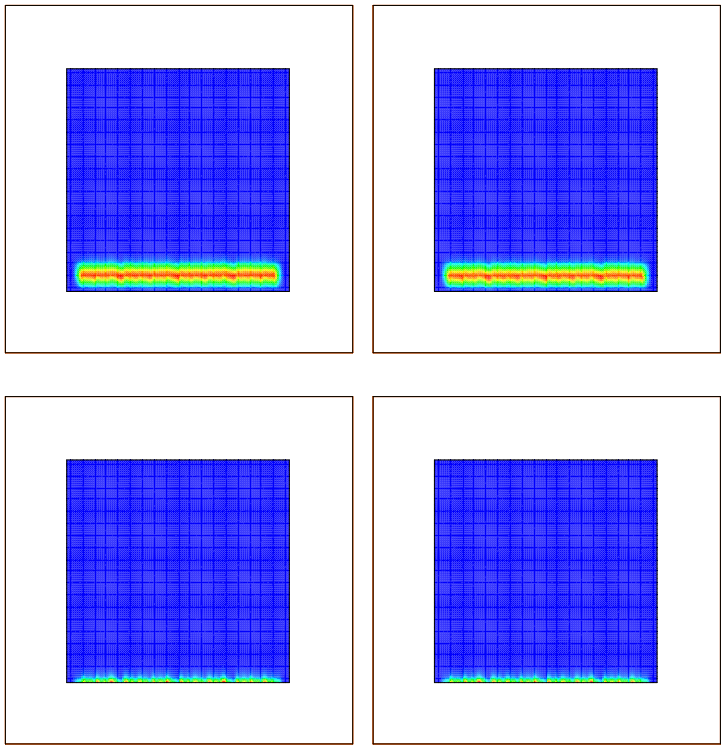

Figure 19: line source, with number of time-steps equal to 25.

In Figure 20, we see the deposition rates of the line source, x is between 5 to 95, and y is between 20 to 30.

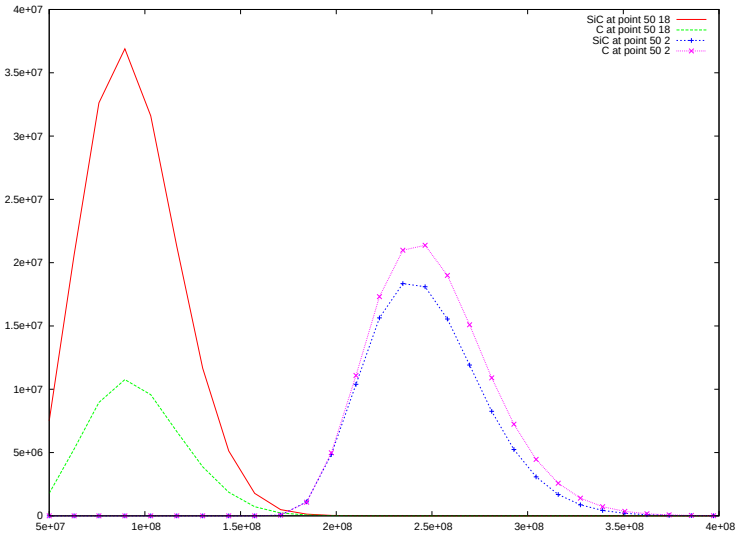

Figure 20: Deposition rates in case of line source, $x \in [5, 95], y \in [20, 25]$.

RATE
$SiC_{source,max} : C_{target,max}$
$1.8.10^7 : 2.2.10^7 = 0.81$

Table 23: Rate of the concentration.

5.3 Test experiment 3: Regression with Temperature and Power

In the next experiment we apply a more flexible approximation method to obtain the parameters of the mathematical method. We apply the regression and can fit to all the physical parameters, because we are not restricted to a given interpolation grid.

The reaction is given as:

$A \to B$ and $B \to C$ and we apply to $2SiC + 4H \to SiC + CH4 + Si$.

We computed the ratio $SiC : C$ for temperatures $T = 400, 600, 800$ and power of the plasma $100, 300, 500, 900$ and fit the given experimented ration with UG program to the mathematical model with the reaction parameter λ.

We used linear regression, see Section 4, and compute λ for the new temperatures $T = 450, 500, 800$ and apply the ratio of the simulated new parameters. This values can be given back to the physical experiments, see Table 24.

T	P	Exact λ	Regression λ	Exact ratio(SiC:C)	Regression ratio(SiC:C)
400	900	1e-09	1.703e-09	1:0.97	0.835
400	500	0.2e-08	2.903e-09	1.3:1	1.616
400	100	0.5e-08	4.103e-09	2.4:1	2.011
600	300	0.25e-08	3.303e-09	1.5:1	1.774
800	500	0.125e-8	2.503e-09	1:1	1.192
800	900	0.175e-8	1.303e-09	1.2:1	1.132
500	500		2.803e-09		1.58
600	600		2.4030e-09		1.433
800	800		1.603-09		1.206
400	400		3.203e-09		1.715
450	450		2.703e-09		1.57
800	100		3.703e-09		1.93

Table 24: Parameter of the source concentration.

One Source

Point source of SiC at the position	$(x, y) = (50, 20)$
Point source of H at the position	$(x, y) = (50, 20)$
Starting point of the source concentration	$t_{start} = 0.0$
End point of the source concentration	$t_{end} = 110^8$
Amount of the permanent source concentration	$c_{source} = 1.0$
Number of time steps	100

Table 25: Parameter of the source concentration.

We take here a points sources.

In Figure 21, we present the concentration of the one point source experiment.

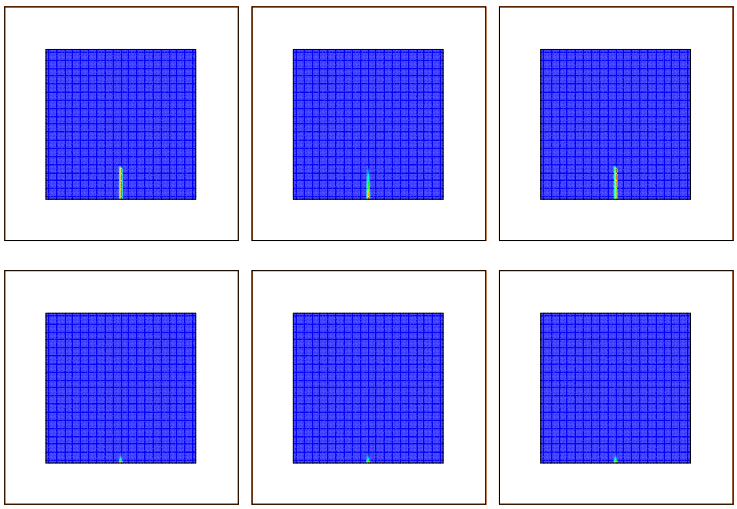

Figure 21: one point source experiment.

In Figure 22, we show the deposition rates of the one point source experiment.

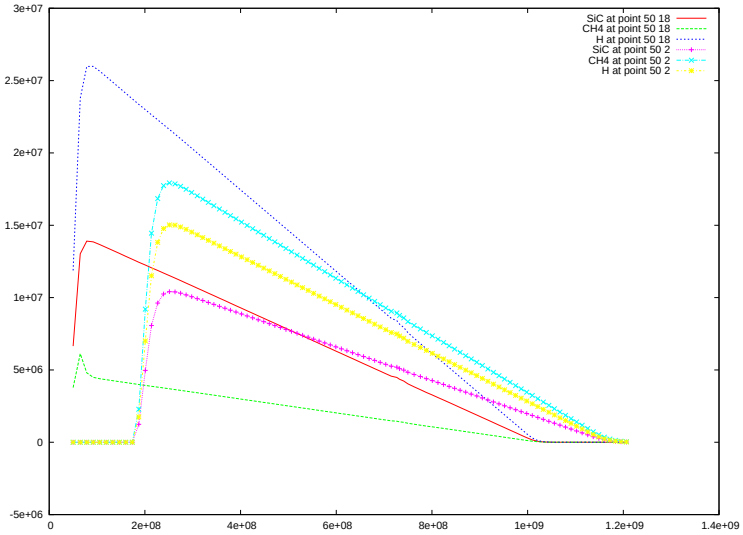

Figure 22: Deposition rates in case of one point source experiment.

RATE
$C_{source,max} : SiC_{target,max}$
$1.8.10^7 : 1.10^7 = 1.8$

Table 26: Rate of the concentration.

Nine Point Sources

Nine point sources of SiC at the position	$(x = 10, 20, 30, 40, 50, 60, 70, 80, 90.y = 20)$
Nine point sources of SiC at the position	$(x = 10, 20, 30, 40, 50, 60, 70, 80, 90.y = 20)$
Starting point of the source concentration	$t_{start} = 0.0$
End point of the source concentration	$t_{end} = 110^8$
Amount of the permanent source concentration	$c_{source} = 1.0$
Number of time steps	25

Table 27: Parameter of the source concentration.

We take here a nine point sources of both concentration.

In Figure 23, we present the concentration of the nine point sources experiment.

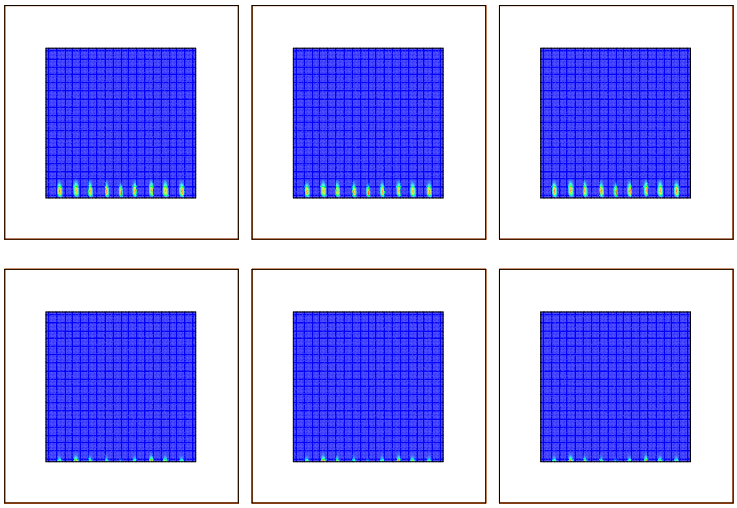

Figure 23: nine point sources experiment.

In Figure 24, we show the deposition rates of the nine point sources experiment.

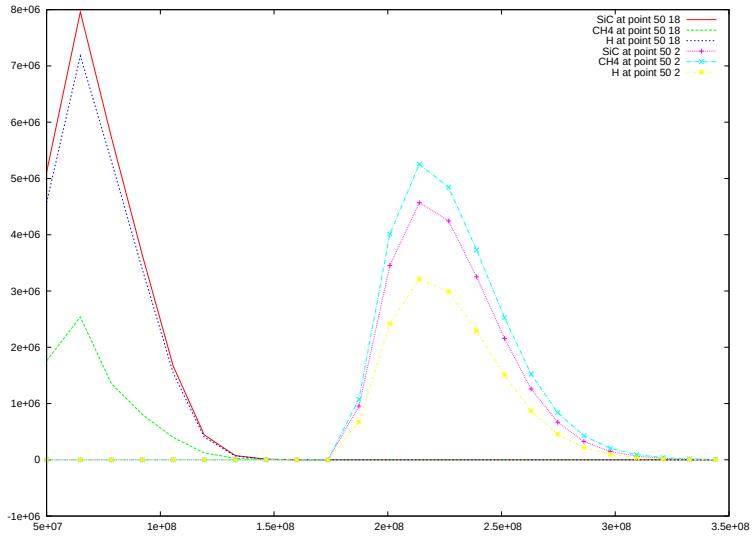

Figure 24: Deposition rates in case of nine point sources experiment.

RATE
$C_{source,max} : SiC_{target,max}$
$5.10^6 : 4.4.10^6 = 1.13$

Table 28: Rate of the concentration.

81 Point Sources, $t_{half} = 2\ 10^8$

In this first experiment,the value of temperature is 400 C and λ is $0.5\ 10^{-8}$.

81 point sources of SiC at the position	$X = 10, 11, 12, 000, 90. Y = 20.$
Line source of H at the position	$x \in [5, 95], y \in [20, 25]$
Starting point of the source concentration	$t_{start} = 0.0$
End point of the source concentration	$t_{end} = 110^8$
Amount of the permanent source concentration	$Sic_{source} = 1.0, H_{source} = 0.20$
Number of time steps	100

Table 29: Parameter of the source concentration.

We take here the concentration of SiC as a point sources, and the concentration of H is a line source.

In Figure 25, we present the concentration of the 81 point sources experiment .

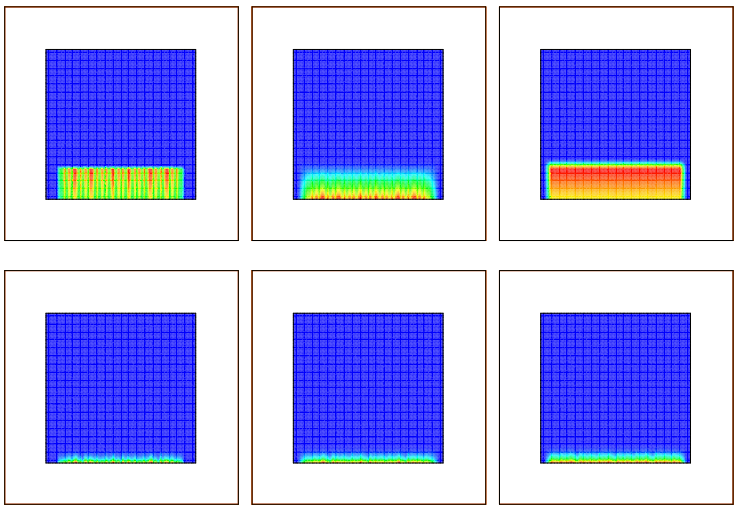

Figure 25: 81 point sources experiment.

In Figure 26, we show the deposition rates of the 81 point sources experiment.

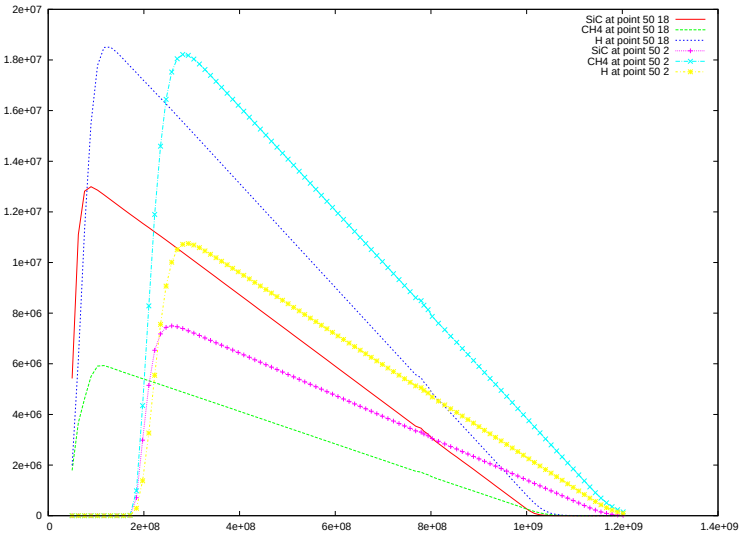

Figure 26: Deposition rates in case of 81 point sources experiment.

RATE
$C_{source,max} : SiC_{target,max}$
$1.8.10^7 : 0.75.10^7 = 2.4$

Table 30: Rate of the concentration.

Remark 7 *The regression method is more flexible for approximating to the physical parameters. We obtain numerical results for different parameter studies, that are fitted to the physical experiments. First test examples with multiple sources and temperature regions which are interested to the physicists are simulated. Here we have coupled a mathematical model with a physical experiment and studied a near region of the deposition process.*

6 CONCLUSIONS

We present numerical simulation for a CVD process to deposit SiC films. Based on the different scales of physical and mathematical experiments, we apply parameter approximation to fit the physical experiment into the mathematical experiment. Numerical approximations to the experimental dates included the new parameters of the mathematical model. Such experiments allow to reduce to a acceptable number of physical experiments and gave engineers and experimentalists a mathematical tool to predict complex physical processes.

First numerical results show predictions of the physical experiments with a transport-reaction equation of the deposition process.

The temperature of the target and power of the plasma are chosen in such manner, where simulation results can help to find an optimal deposition. Furthermore multiple source obtain best results in a homogeneous layer deposition.

Such numerical simulations help to predict the deposition rates of the underlying film, e.g., SiC. In future, we will analyze the validity of the models with more complicate precursor gases. Here the outstanding of multivariate analysis will be important to approximate a large number of parameters.

REFERENCES

Barsoum MW and El-Raghy T (1996). Synthesis and characterization of a remarkable ceramic: ti_3sic_2. *J.Am.Ceram.Soc. 79*(1), pp. 1953–1956.

Bastian, P Birken K Eckstein K Johannsen K Lang S Neuss N and Rentz-Reichert H (1997).

Ug-a flexible software toolbox for solving partial differential equations. *Computing and Visualization in Science 1*(1), pp. 27–40.

Bear J (1972). *Dynamics of fluids in porous media*. American Elsevier, New York.

Burlisch R and Stoer J (2002). *Introduction to Numerical Analysis*. Springer Verlag. Third Edition.

Cao, GZ Brinkman H Meijerink J DeVries KJ and Burggraaf AJ (1993). Kinetic study of the modified chemical vapour deposition process in porous media. *J.Mater.Chem. 3*(12), pp. 1307–1311.

Chapman B (1980). *Glow Discharge Processes. Sputering and Plasma Etching*. John Wiley & Sons, Inc. First Edition.

Dobkin MK and Zuraw DM (2003). *Principles of Chemical Vapor Deposition.* Springer, New York. First Edition.

Favia, P Sardella E Gristina R. Millella A and D'Agostino R (2002). Functionalization of biomedical polymers by means of plasma processes: Plasma treated polymers with limited hydrophobic recovery and pe-cvd of cooh functional coatings. *Journal of Polymer Science and Technology 15*(2), pp. 341–350.

Frolkovič P (2002). Flux-based method of characteristics for contaminant transport in flowing groundwater. *Computing and Visualization in Science*.

Frolkovič P and De Schepper H (2001). Numerical modelling of convection dominated transport coupled with density driven flow in porous media. *Advances in Water Resources 24*.

Frolkovič P and Geiser J (2003). Discretization methods with discrete minimum and maximum property for convection dominated transport in porous media.

Geiser J (2003). *Gekoppelte Diskretisierungsverfahren für Systeme von Konvektions-Dispersions-Diffusions-Reaktionsgleichungen.* Ph. D. thesis, Universität Heidelberg.

George P (2008). *Chemical Vapor Deposition: Simulation and Optimization*. VDM Verlag Dr. Müller, Saarbrücken, Germany. First Edition.

Glowinski R (2003). *Numerical methods for fluids.* Handbook of Numerical Analysis, Gen. eds. P.G. Ciarlet, J. Lions, Vol. IX, North-Holland Elsevier, Amsterdam, The Netherlands.

Gobbert MK and Ringhofer CA (1998). An asymptotic analysis for a model of chemical vapor deposition on a microstructured surface. *SIAM Journal on Applied Mathematics. 58*.

Higashi K and Pigford ThH (1980). Analytical models for migration of radionuclides in geologic sorbing media. *Journal of Nuclear Science and Technology 17(9)*.

Hlavacek, V Thiart J and Orlicki D (1995). Morphology and film growth in cvd reactions. *J. Phys. IV France 5*.

Johannsen K (1999). *Robuste Mehrgitterverfahren für die Konvektions-Diffusions Gleichung mit wirbelbehafteter Konvektion*. Ph. D. thesis, University of Heidelberg, Germany.

Jury WA and Roth K (1990). *Transfer Functions and Solute Movement through Soil*. Basel, Boston, Berlin: Bikhäuser Verlag.

Kadetov VA (2004). *Diagnostics and modeling of an inductively coupled radio frequency discharge in hydrogen*. Ph. D. thesis, Ruhr Universität Bochum.

Leveque RJ (2002). *Finite Volume Methods for Hyperbolic Problems.* Cambridge Texts in Applied Mathematics, Cambridge, UK.

Lieberman MA and Lichtenberg AJ (2005). *Principle of Plasma Discharges and Materials Processing.* Wiley-Interscience, AA John Wiley & Sons, Inc Publication. second Edition.

Morosoff N (1990). *Plasma Deposition, Treatment and Etching of Polymers*. R. d'Agostino ed., Acad. Press. First Edition.

Neil T.H (2002). *Applied Multivariate Analysis*. Springer, Berlin New York.

Ohring M (2002). *Materials Science of Thin Films.* Academic Press, San Diego, New York, Boston, London. Second Edition.

Rouch H (2006). Mocvd research reactor simulation. *Proceedings of the COMSOL Users Conference 2006 Paris*, Paris, France.

Scheidegger AE (1961). General theory of dispersion in porous media. *Journal of Geophysical Research 66*.

Senega TK and Brinkmann RP (2006). A multi-component transport model for non-equilibrium low-temperature low-pressure plasmas. *J. Phys. D: Appl.Phys. 39*.